coatings

MDPI

Article

Theoretical Studies of the Adsorption and Migration Behavior of Boron Atoms on Hydrogen-Terminated Diamond (001) Surface

Xuejie Liu *, Congjie Kang, Haimao Qiao, Yuan Ren, Xin Tan and Shiyang Sun

School of Mechanical Engineering, Inner Mongolia University of Science & Technology, Baotou, Inner Mongolia 014010, China; happykcj@163.com (C.K.); 15540153167@163.com (H.Q.); renyuan_bt@126.com (Y.R.); heart_tan@126.com (X.T.); sunshy@imust.cn (S.S.)

* Correspondence: xuejieliu2000@yahoo.com; Tel./Fax: +86-472-595-2268

Academic Editors: Quanshun Luo and Yongzhen Zhang

Received: 20 March 2017; Accepted: 20 April 2017; Published: 27 April 2017

Abstract: The adsorption and migration activation energies of boron atoms on a hydrogen-terminated diamond (001) surface were calculated using first principles methods based on density functional theory. The values were then used to investigate the behavior of boron atoms in the deposition process of B-doped diamond film. On the fully hydrogen-terminated surface, the adsorption energy of a boron atom is relatively low and the maximum value is 1.387 eV. However, on the hydrogen-terminated surface with one open radical site or two open radical sites, the adsorption energy of a boron atom increases to 4.37 eV, and even up to 5.94 eV, thereby forming a stable configuration. When a boron atom deposits nearby a radical site, it can abstract a hydrogen atom from a surface carbon atom, and then form a BH radical and create a new radical site. This study showed that the number and distribution of open radical sites, namely, the adsorption of hydrogen atoms and the abstraction of surface hydrogen atoms, can influence the adsorption and migration of boron atoms on hydrogen-terminated diamond surfaces.

Keywords: B-doped diamond films; adsorption energy; migration behavior; first principles methods

1. Introduction

Boron-doped diamond (BDD) films deposited by chemical vapor deposition (CVD) have attracted increasing research attentions owing to their outstanding properties, including mechanical and electrochemical stability, as well as a wide potential window, low and stable background current, good biocompatibility, high corrosion resistance, and high efficiency in electrochemical oxidation processes. BDD films have been used in a number of electrochemical applications, such as water treatment, electro-synthesis, electro-catalysis, electro-analytical measurement, electrochemical energy technology, and biosensing [1–6], and BDD depositions have also been employed to prepare smooth coatings for machining carbon fiber reinforced plastics [7]. BDD film-coated rectangular-hole-shaped drawing dies have been discovered to not only display much better adhesion and wear-resistant properties, but also have higher initial surface smoothness before polishing and relatively lower film hardness, making it liable to be polished to the appropriate surface smoothness [8]. The performances of BDD films depend heavily on the films' microstructure, which mainly relies on the formation mechanism of BDD films in the CVD process. Therefore, the surface chemical process involved in the CVD diamond and BDD film growth has been extensively investigated [9–15]. With the method used to investigate the surface migration in diamond growth [10–13] and the insertion of boron into methane [16], Ashfold's group studied boron doping during diamond CVD, including boron addition to the cluster surface, boron insertion into the diamond surface, boron loss processes from the diamond surface [14], B and BH insertion reactions, and BH migration on the diamond surface [15].

In the present research, the diamond (001) surface plane is considered, because the (001) plane is one of most frequently obtained surface planes in CVD-grown crystalline diamond. Further, the {100} diamond exhibits a cubic morphology, with smooth, flat crystallite surfaces, and low defect densities, ensuring that {100} growth has long been a focus of experimental and theoretical study [11,17,18].

The method employed in the present work is slightly different from those of the previous studies [10–16]. First, a relatively large slab model 4 × 4 × (8 + 1 + 8) was employed as a hydrogen-terminated diamond (001) surface model. Second, the adsorption energies of an atom at certain highly symmetrical positions on the diamond (001) surface were calculated. Third, the potential energy surface (PES) was displayed using the calculated adsorption energy values. Fourth, the migration path was determined by analyzing the PES. Fifth, several image atoms were set along the migration path. Sixth, the minimum energies along the migration path were calculated using the nudged elastic band (NEB) method [19], and the saddle point energy or the energy barrier was then determined.

According to the gas-phase chemistry and composition in microwave plasma activated $B_2H_6/Ar/H_2$ mixtures [20,21], boron atoms are the most abundant gas-phase BH_x species adjacent to the growing diamond surface. Plasma field research [22] indicated that a great amount of hydrogen atoms exist on the substrate surface in a hydrogen-rich diamond deposition. As a result, the adsorption of hydrogen atoms and the abstraction of surface hydrogen atoms play important roles in the diamond growth process [10,23]. Therefore, the present study focused on the adsorption and migration behavior of boron atoms on a hydrogen-terminated diamond (001) surface. The investigation focused on boron atoms on a fully hydrogen-terminated surface and boron atoms on hydrogen-terminated surfaces with one and two open radical sites.

2. Calculation Details

Calculations were performed using a Vienna Ab-Initio Simulation Package (VASP) (VASP5.2, University Wien, Wien, Austria) code [24–26], which was based on density functional theory. In specific calculations, a plane-wave basis was set and periodic boundary conditions were used to determine the Kohn–Sham ground state. The projector-augmented wave (PAW) method [27,28] was used to describe electronic and ionic interactions. Local density was described with generalized gradient approximation (GGA) based on the Perdew-Burke-Ernzerhof (PBE) formulation [29,30]. Electron and ion relaxation convergence precisions were 10^{-4} and 10^{-3} eV, respectively. The Brillouin zone was sampled using the Monkhorst-Pack k-point grid [31] during a self-consistent calculation to identify the electronic ground state. A 5 × 5 × 1 k-point mesh was utilized for slab calculations. The parameter settings were optimized for the calculations. Moreover, spin-polarized calculations were performed to optimize the structure and configuration. The NEB method in VASP [19] was used to calculate the minimum migration energy of atoms on the hydrogen-terminated diamond (001) surface.

Prior to calculating atom migration, a lattice constant of 0.3568 nm was determined by adjusting the calculation parameters to optimize the diamond crystalline structure, in which the plane-wave cut-off energy was 350 eV. The calculated lattice constant was close to the experimental value of 0.3567 nm. A 4 × 4 × (8 + 1 + 8) slab composed of eight carbon layers (with 16 carbon atoms per plane), one hydrogen layer, and eight vacuum layers was used to model the hydrogen-terminated diamond (001) film, as shown in Figure 1. The height of the vacuum layer was approximately 0.8020 nm, and a periodically arranged interference was prevented. The hydrogen-terminated diamond (001) film model was selected because of the abutment of hydrogen atoms on the surface in the diamond film synthesis [22]. During relaxation, the three bottom layers of carbon atoms were fixed, whereas the others moved freely. After relaxation, the hydrogen-terminated diamond (001) surface underwent reconstruction. The length of the dimer bond was 0.162 nm, the bond length between the surface carbon atom and the hydrogen atom was 0.102 nm, and the total energy of the configuration was −1164.233 eV.

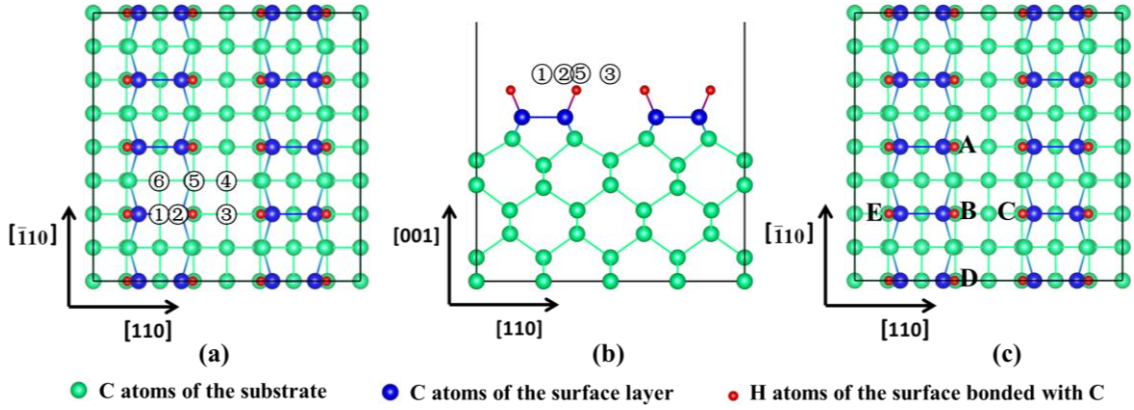

Figure 1. Six highly symmetrical positions and the open radical sites on the reconstructed hydrogen-terminated diamond (001) slab: (**a**) main view; (**b**) top view; (**c**) The open radical sites: when Hydrogen B was abstracted, the configuration represented the model of a hydrogen-terminated diamond (001) slab with one open radical site, denoted as 1ORS; when Hydrogens A and B were abstracted, the configuration stood for the model with two open radical sites along the dimer row, denoted as 2ORS-R; when Hydrogens B and C were abstracted, the configuration represented the model with two open radical sites along the dimer chain by the open-ring side, denoted as 2ORS-CO; when Hydrogens E and B were abstracted, the configuration represented the model with two open radical sites along the dimer chain by the close-ring side, denoted as 2ORS-CC.

Energies of a single carbon atom and a single boron atom were determined (Table 1) by fitting the calculated cohesive energy with the experimental value. The calculated lattice constant and cohesive energy were consistent with experimental values. Thus, our calculations are reasonable and reliable for studying the adsorption and migration behaviors in this system.

Table 1. Lattice constants and cohesive energies of C and B, and energies of a single C atom and a single B atom.

Items	C Atom [32]	B Atom
Energy of single atom (eV)	−1.479	−0.324
Lattice from calculation (nm)	0.3568	0.181
Lattice from experiment (nm) [33]	0.3567	0.177
Difference in the percentage of lattice (%)	0.028	2.26
Cohesive energy from calculation (eV·atom^{-1})	7.626	5.96
Cohesive energy from experiment (eV·atom^{-1}) [33]	7.37	5.81
Difference in the percentage of cohesive energy (%)	3.47	2.58

Adsorption and migration behaviors of a single boron atom on the hydrogen-terminated diamond (001) surface were investigated. Based on the special structure of the diamond, six highly symmetrical positions existed on the reconstruction surface of hydrogen-terminated diamond (001), as shown in Figure 1a,b: (1) on the bridge site of the dimer ring-closing bond (denoted as P1); (2) on top of the carbon atom in the carbon dimer (denoted as P2); (3) at the bridge site of the dimer ring-opening bond (denoted as P3); (4) between the carbon dimer row located on top of the atom in the third layer (denoted as P4); (5) between the carbon dimer on top of the atom in the second layer (denoted as P5); and (6) between the carbon dimer on top of the atom in the third layer (denoted as P6). A single boron atom was set at each of the six positions (0.2 nm higher than the surface layer) for calculating the adsorption energy of a boron atom. The orientations of [$\bar{1}$10] and [110] were regarded as the dimer row and the dimer chain, respectively [10]. The open radical sites on the hydrogen-terminated diamond surface are shown in Figure 1c. When Hydrogen B was abstracted, the configuration represented the model of a hydrogen-terminated diamond (001) slab with one open radical site (denoted as 1ORS); when

Hydrogen A and B were abstracted, the configuration stood for the model with two open radical sites along the dimer row (denoted as 2ORS-R); when Hydrogens B and C were abstracted, the configuration represented the model with two open radical sites along the dimer chain by the ring-opening side (denoted as 2ORS-CO); and when Hydrogens E and B were abstracted, the configuration represented the model with two open radical sites along the dimer chain by the ring-closing side (denoted as 2ORS-CC).

3. Results and Discussion

3.1. Adsorption of a Single Boron Atom on a Fully Hydrogen-Terminated Diamond (001) Surface

The total energies of configurations were calculated to obtain the adsorption energies of the boron atom at the six highly symmetrical positions. The adsorption energy is defined as

$$E_{ad} = -(E_{tot} - E_{slab} - E_B) \quad (1)$$

where E_{tot} is the total energy of configuration with adsorbed atoms, E_{slab} is the total energy of the relaxation hydrogen-terminated diamond (001) slab without adsorbed atoms, and E_B is the energy of a single boron atom. The total energy of the hydrogen-terminated diamond (001) slab E_{slab} was −1164.233 eV.

The total energies and adsorption energies of a single boron atom on the hydrogen-terminated diamond (001) surface are listed in Table 2. At P4 and P6, the boron atom desorbed. At P1, P2, and P3, the distance between the boron atom and the surface carbon atoms was approximately 0.289–0.354 nm, which is much longer than the covalent radius sum of the boron atom and the carbon atom (i.e., 0.165 nm). Thus, the boron atom could not bond with the surface carbon atoms. Moreover, the adsorption energies were relatively low (0.08–0.162 eV). At P5, both distances between the boron atom and two surface carbon atoms were 0.158 nm, and the distance between the boron atom and the carbon atom in the second layer was 0.145 nm. These three bond lengths are all close to the covalent radius sum of the boron atom and the carbon atom, i.e., 0.165 nm. Obviously, the boron atom bonded with these three carbon atoms; thus, the adsorption energy reached the maximum value of 1.378 eV.

Table 2. Total energies and adsorption energies of a single boron atom on a fully hydrogen-terminated diamond (001) surface.

Position	P1	P2	P3	P4	P5	P6
E_{tot} (eV)	−1164.719	−1164.640	−1164.717	−1166.029	−1165.935	−1172.714
E_{ad} (eV)	0.162	0.083	0.160	(desorption)	1.378	(desorption)

The adsorbed boron atom could migrate along the path from P5 to P1 and further to another P5. The migration energies along the path were calculated using the NEB method in the VASP code. The calculation results are listed in Table 3. The minimum energy data indicate that the migration barrier along the path is 1.216 eV. Therefore, the boron atom migration along the path is easy at normal CVD diamond film deposition temperature (700–900 °C).

Table 3. Minimum energies during the migration of a single boron atom on a fully hydrogen-terminated diamond (001) surface.

Position	P5	I	II	III	IV	P1
E_{tot} (eV)	−1165.935	−1165.543	−1164.879	−1164.893	−1164.919	−1164.719
E_{ad} (eV)	1.378	0.986	0.322	0.336	0.362	0.162

3.2. Adsorption of a Single Boron Atom on a Hydrogen-Terminated Diamond (001) Surface with One Open Radical Site

When Hydrogen B was abstracted Figure 1c, the configuration represented the model of a hydrogen-terminated diamond (001) slab with one open radical site (denoted 1ORS). The charge analysis shows that when a hydrogen atom bonded with the surface carbon atom (C_{NN}) was removed, the total magnetic moment of C_{NN} changed from 0.000 to 0.412 μ_B, implying that the C_{NN} had unpaired electrons and was more reactive. The total energy of the configuration of 1ORS E_{slab} is −1158.567 eV. The total energies of the configurations were calculated to study the adsorption of a boron atom at the six symmetrical positions. The relevant adsorption energies were obtained using Equation (1). The total energies and adsorption energies of a single boron atom on the hydrogen-terminated diamond (001) surface with one open radical site are listed in Table 4, and the PES of the adsorption energies is displayed in Figure 2.

Table 4. Total energies and adsorption energies of a single boron atom on a hydrogen-terminated diamond (001) surface with one open radical site.

B-Igration	P1	P2	P3	P4	P5	P6
E_{tot} (eV)	−1163.260	−1162.551	−1161.086	−1159.741	−1164.087	−1160.106
E_{ad} (eV)	4.370	3.661	2.196	0.851	5.197	1.216

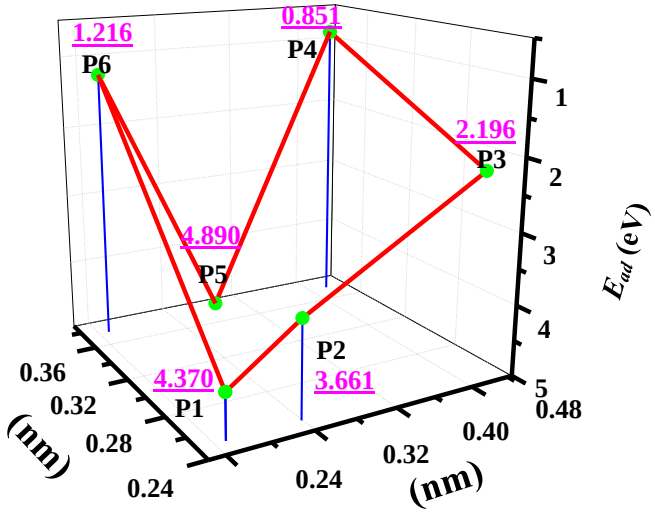

Figure 2. Potential energy surface (PES) of a single boron atom on a hydrogen-terminated diamond (001) surface with one open radical site.

Given that Hydrogen B was abstracted, the boron atom deposited at P2 could bond with the surface carbon atom; the bond length was approximately 0.154 nm, which is slightly less than their covalent radius sum of 0.165 nm. Thus, the adsorption energy reached the relatively large value of 3.66 eV. When the boron was deposited at P1, the boron atom bonded with the surface carbon dimer with bond lengths 0.152 and 0.142 nm, and the dimer bond was broken. The Bader charge analysis indicates that the charge of boron atom reduces from 2.823 to 1.555 electrons; the charge of two carbon atoms increase from 3.957 to 4.676 electrons and from 4.104 to 4.908 electrons. Thus, the adsorption energy increased to 4.37 eV, which was close to the result in previous study [15], which is 363 kJ/mol. When the boron atom was deposited at P5, the boron atom abstracted the hydrogen atom from a carbon atom nearby and bonded with two surface carbon atoms with bond lengths both at 0.159 nm. The boron atom bonded also with the carbon atom in the second layer with bond length of 0.185 nm. Therefore, the adsorption energy reached the maximum value of 5.197 eV. At P3, P4, and P6, the

distance between the boron atom and the carbon atom with a dangling bond was relatively large, resulting in low adsorption energies.

The migration path can be determined by analyzing the PES. The boron atom could migrate from P1 to P5. At P5, the boron atom abstracted a hydrogen atom, and then the BH radical could migrate from P5 to P1. Along the migration path, the minimum energies were calculated with the NEB method. The calculation results are listed in Table 5 and the minimum energy path curves are presented in Figure 3a,b. The curve in Figure 3a shows that the boron atom migration from P1 to P5 is difficult, because of a high energy barrier of 2.36 eV. Once the boron atom overcomes the energy barrier, it can abstract the hydrogen atom from the nearby carbon atom and form a BH radical. The curve in Figure 3b shows that the migration of the BH radical is easy because of a low energy barrier of 1.53 eV. However, the BH radical tends to slide back to P5 and forms a stable configuration. The energy barrier for the BH radical to slide back to P5 is 0.017 eV.

Table 5. Minimum energies during the migration of a single boron atom or the BH on the hydrogen-terminated diamond (001) surface with one open radical site.

B-Migration	**P1**	**I**	**II**	**III**	**IV**	**P5**	E_a **(eV)**
E_{tot} (eV)	−1163.260	−1163.103	−1162.575	−1162.217	−1161.725	−1164.087	2.362
ΔE (eV)	0.827	0.984	1.512	1.870	2.362	0	
BH-Migration	**P5**	**I**	**II**	**III**	**IV**	**P1**	E_a **(eV)**
E_{tot} (eV)	−1164.087	−1163.855	−1163.240	−1162.626	−1162.558	−1162.575	1.529
ΔE (eV)	0	0.232	0.847	1.461	1.529	1.512	

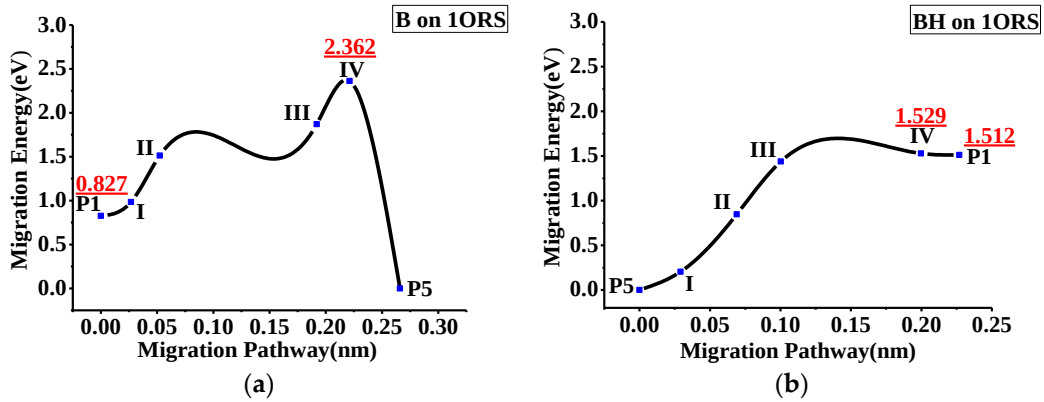

Figure 3. Migration minimum energy path curves of the boron atom and the BH radical on the 1ORS: (**a**) the boron atom migration from P5 to P1 and (**b**) the BH radical migration from P5 to P1.

3.3. Adsorption and Migration Behaviors of a Boron Atom on the Hydrogen-Terminated Diamond (001) Surface with Two Open Radical Sites

As shown in Figure 1c, when Atoms A and B were abstracted, the configuration represented the model of a hydrogen-terminated diamond (001) slab with two open radical sites along the dimer row (denoted as 2ORS-R). The total energy of the configuration of 2ORS-R E_{slab} is −1152.921eV. The total energies of the configurations of a single boron atom on 2ORS-R were calculated to study the adsorption of a boron atom at the six symmetrical positions. The relevant adsorption energies were obtained using Equation (1). The total energies and adsorption energies of a single boron atom on the hydrogen-terminated diamond (001) surface with two open radical site are listed in Table 6 and the PES of the adsorption energies is displayed in Figure 4a–c.

Table 6. Total energies and adsorption energies of a single boron atom on the hydrogen-terminated diamond (001) surface with two open radical sites.

2ORS-R	**P1**	**P2**	**P3**	**P4**	**P5**	**P6**
E_{tot} (eV)	−1157.594	−1156.973	−1158.131	−1155.112	−1159.184	−1155.899
E_{ad} (eV)	4.346	3.725	4.883	1.864	5.936	2.651
2ORS-CO	**P1**	**P2**	**P3**	**P4**	**P5**	**P6**
E_{tot} (eV)	−1157.692	−1156.867	−1158.499	−1154.609	−1158.435	−1154.403
E_{ad} (eV)	4.489	3.664	5.296	1.406	5.232	1.200
2ORS-CC	**P1**	**P2**	**P3**	**P4**	**P5**	**P6**
E_{tot} (eV)	−1159.006	−1157.629	−1158.042	−1154.527	−1158.514	−1155.008
E_{ad} (eV)	4.886	3.509	3.922	0.407	4.396	0.888

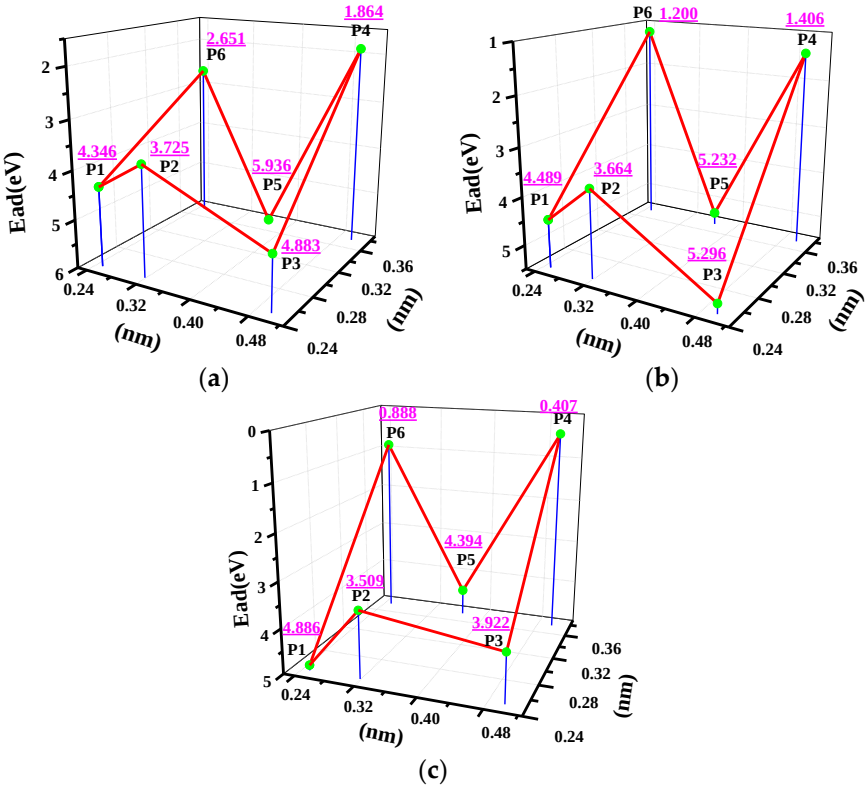

Figure 4. PES of a single boron atom on the hydrogen-terminated diamond (001) surface with two open radical sites: (**a**) on the 2ORS-R; (**b**) on the 2ORS-CO; and (**c**) on the 2ORS-CC.

Given that Atoms A and B were abstracted (Figure 1c), the boron atom deposited at P5 could bond with two carbon atoms on the surface, both with bond lengths of 0.152 nm, which is less than their covalent radius sum of 0.165 nm. In addition, the boron atom bonded with the carbon atom in the second layer, with a bond length of 0.169 nm. Therefore, the adsorption energy reached the maximum value of 5.936 eV. When deposited at P3, the boron atom abstracted a hydrogen atom from the nearby carbon atom and formed a BH radical. The boron atom bonded with two surface carbon atoms and both bond lengths were 0.171 nm. Thus, the adsorption energy reached 4.88 eV. Figure 4a represents the PES with three basins, which were used to determine the migration path. One path is for the boron atom to migrate from P1 to P5 and further to P1′; another path is for the boron atom to migrate from P5 to P3. At P3, the boron atom abstracted a hydrogen atom and formed a BH radical. After that, the BH radical can migrate from P3 to P5.

In the configuration of 2ORS-CO, hydrogen B and C were abstracted (Figure 1c). The boron atom deposited at P3 bonded with two surface carbon atoms, both with bond lengths of 0.158 nm. The adsorption energy reached the maximum value of 5.296 eV. The boron atom deposited at P5 could abstract a hydrogen atom from the nearby surface carbon atom and form a BH radical. The boron atom bonded also with two surface carbon atoms with bond lengths of 0.164 nm and 0.157 nm. In addition, the boron atom bonded with the carbon atom in the second layer, with bond length 0.183 nm. Thus, the adsorption energy was 5.23 eV. The migration path can be determined by analyzing the PES in Figure 4b. One path is for the boron atom to migrate from P3 to P1 and further to P3′; another path is for the BH radical to migrate from P5 to P3.

When Hydrogen B and E were abstracted (Figure 1c), the boron atom deposited at P1 could bond with the surface carbon dimer, both with bond lengths of 0.1478 nm, which is less than their covalent radius sum of 0.165 nm; in addition, the dimer bond was broken. Therefore, the adsorption energy reached the maximum value of 4.886 eV. The boron atom deposited at P3 abstracted a hydrogen atom from a carbon atom nearby and formed a BH radical. The boron atom bonded also with two surface carbon atoms with bond lengths of 0.171 nm and 0.172 nm. Thus, the adsorption energy reached 3.922 eV. Similar to the case of 2ORS-CO, the boron atom at P5 abstracted a hydrogen atom from the nearby surface carbon atom and formed a BH radical. The boron atom bonded with two surface carbon atoms with bond lengths of 0.160 nm and 0.158 nm. Moreover, the boron atom bonded with the carbon atom in the second layer with a bond length of 0.184 nm. Hence, the adsorption energy reaches 5.23 eV. The migration path can be determined by analyzing the PES in Figure 4c. One path is for the boron atom to migrate from P1 to P3; another path is for the BH radical to migrate from P3 to P1. The third path, similar to the case of 2ORS-CO, is for the BH radical from P5 to P1.

The migration energies along the path were calculated using the NEB method in the VASP code. The calculation results are listed in Table 7, and the minimum energy path curve is presented in Figure 5. The minimum energy path curve in Figure 5a shows a deep basin between two shallow basins. The boron atom on the configuration of 2ORS-R will slide to a shallow basin and overcomes an energy barrier of 0.54 eV from P1 to P5. However, the migration energy barrier of the boron atom from P5 to P1 is 1.71 eV. The energy barrier of the boron atom from P5 to P3 is 1.94 eV (Figure 5b). At P3, the boron atom abstracted a hydrogen atom and formed a BH radical. The migration of the BH radical from P3 to P5 is very easy because of the low energy barrier of 0.74 eV, as shown in Figure 5c.

The migration of a boron atom in the 2ORS-CO configuration along the path P1 to P3 (Figure 5d) is easy because of the low energy barrier of 0.825 eV. The return migration from P3 to P1 requires 1.632 eV to overcome the energy barrier. The migration of a BH radical in the 2ORS-CO configuration along the path from P5 to P3 is easy, given the low energy barrier of 0.765 eV, as shown in Figure 5e.

The migration of a boron atom in the 2ORS-CC configuration along the path P1 to P3 is relatively difficult because the energy barrier is high, i.e., 2.557 eV (Figure 5f). At P3, the boron atom abstracted a hydrogen atom and formed a BH radical. The migration of the BH radical from P3 to P1 (Figure 5g) needs to overcome an energy barrier of 1.882 eV. The migration of a BH radical in the 2ORS-CC configuration along the path from P5 to P1 is similar to that in the 2ORS-CO configuration.

The analyses of the PES and the migration of a boron atom in 2ORS-R, 2ORS-CO, and 2ORS-CC configurations indicate that the adsorption of a boron atom at two open radical sites forms a stable configuration and the adsorption energies are from 3.922 to 5.936 eV. All PES for the 2ORS-R, 2ORS-CO, and 2ORS-CC configurations represent the multiple-basin shapes. Moreover, the boron atom nearby the radical site could abstract a hydrogen atom from the surface carbon atom, form a BH radical, and create a new radical site.

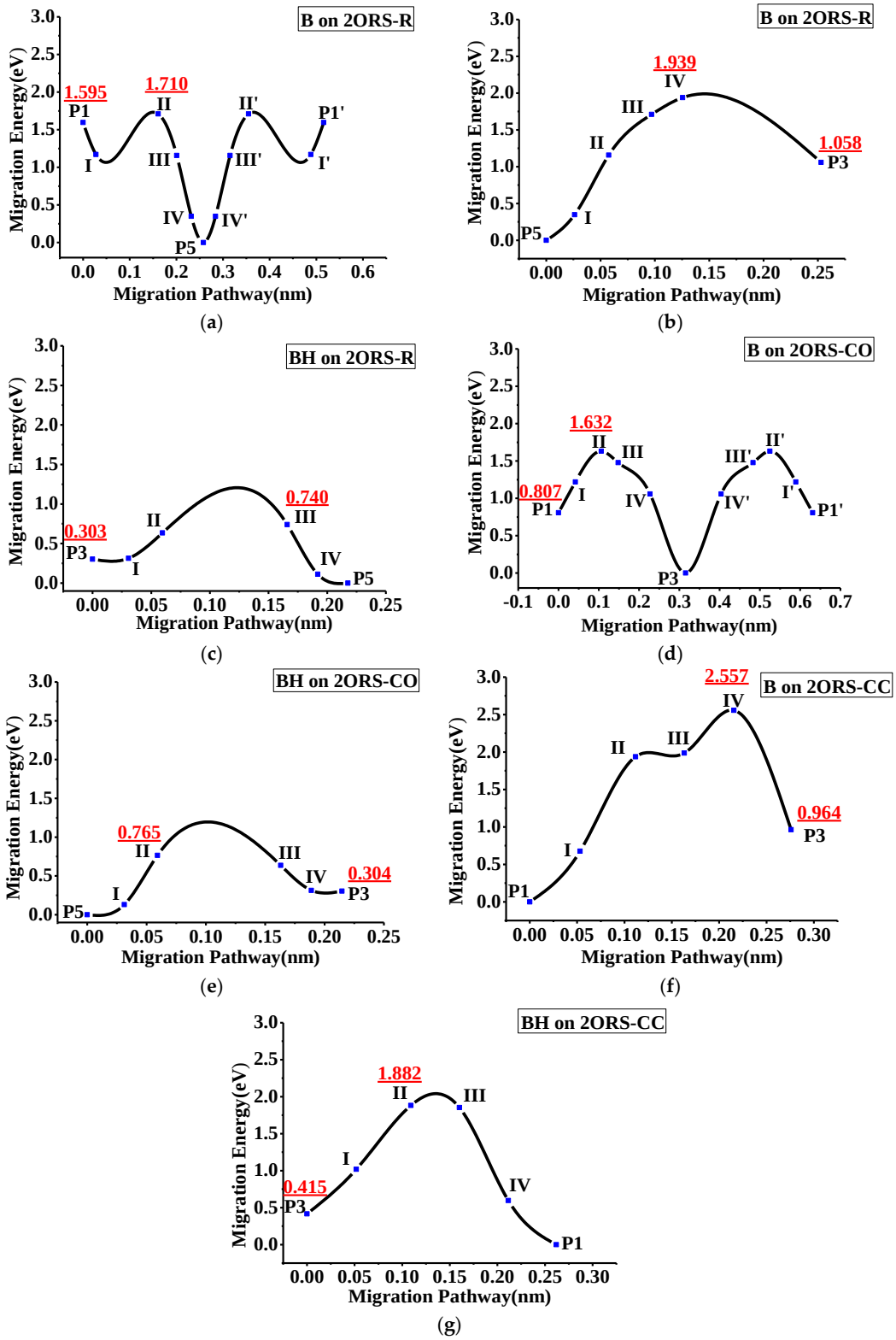

Figure 5. Minimum energy path curves for the boron (B) atom or the BH radical on the hydrogen-terminated diamond (001) surface with two open radical sites: (**a**) B migration from P1 to P5 on 2ORS-R; (**b**) B migration from P5 to P3 on 2ORS-R; (**c**) BH migration from P3 to P5 on 2ORS-R; (**d**) B migration from P1 to P3 on 2ORS-CO; (**e**) BH migration from P5 to P3 on 2ORS-CO; (**f**) B migration from P1 to P3 on 2ORS-CC; (**g**) BH migration from P3 to P1on 2ORS-CC.

Table 7. Minimum energies during the migration of a single B atom on the hydrogen-terminated diamond (001) surface with two open radical sites.

2ORS-R	**P1**	**I**	**II**	**III**	**IV**	**P5**	E_a **(eV)**
E_{tot} (eV)	−1157.594	−1158.018	−1157.479	−1158.032	−1158.841	−1159.189	1.710
ΔE (eV)	1.595	1.171	1.710	1.157	0.348	0	
2ORS-R	**P5**	**I**	**II**	**III**	**IV**	**P3**	E_a **(eV)**
E_{tot} (eV)	−1159.189	−1158.841	−1158.032	−1157.479	−1157.259	−1158.131	1.939
ΔE (eV)	0	0.348	1.157	1.71	1.939	1.058	
2ORS-R (B H)	**P3**	**I**	**II**	**III**	**IV**	**P5**	E_a **(eV)**
E_{tot} (eV)	−1158.131	−1158.121	−1157.800	−1157.694	−1158.321	−1158.434	0.740
ΔE (eV)	0.303	0.313	0.634	0.740	0.113	0	
2ORS-CO	**P1**	**I**	**II**	**III**	**IV**	**P3**	E_a **(eV)**
E_{tot} (eV)	−1157.692	−1157.280	−1156.867	−1157.022	−1157.441	−1158.499	1.632
ΔE (eV)	0.807	1.219	1.632	1.477	1.058	0	
2ORS-CO(BH)	**P5**	**I**	**II**	**III**	**IV**	**P3**	E_a **(eV)**
E_{tot} (eV)	−1158.435	−1158.322	−1157.670	−1157.799	−1158.121	−1158.131	0.765
ΔE (eV)	0	0.131	0.765	0.636	0.314	0.304	
2ORS-CC	**P1**	**I**	**II**	**III**	**IV**	**P3**	E_a **(eV)**
E_{tot} (eV)	−1159.006	−1158.329	−1157.069	−1157.020	−1156.449	−1158.042	2.557
ΔE (eV)	0	0.667	1.937	1.986	2.557	0.964	
2ORS-CC(BH)	**P3**	**I**	**II**	**III**	**IV**	**P1**	E_a **(eV)**
E_{tot} (eV)	−1158.042	−1157.438	−1156.575	−1156.604	−1157.860	−1158.457	1.882
ΔE (eV)	0.415	1.019	1.882	1.853	0.597	0	

4. Conclusions

In this study, the adsorption and migration activation energies of a single boron atom on a full hydrogen-terminated diamond (001) surface and on the hydrogen-terminated diamond (001) surface with several open radical sites were systematically investigated using first principles methods. The following conclusions can be drawn from the results:

1. On the fully hydrogen-terminated diamond surface, the adsorption energies of a boron atom are small and the maximum value is 1.387 eV. The migration barrier of the boron atom is 1.216 eV. Thus, boron atom migration on the surface is easy at the CVD diamond deposition temperature (700–900 °C).
2. On the hydrogen-terminated diamond surface with one open radical site or two open radical sites, the adsorption energies of a boron atom increase to 4.37 eV, even up to 5.94 eV, thereby forming a stable configuration. All PES on the hydrogen-terminated diamond surface with two open radical sites represent the multiple-basin shapes. Thus, a boron atom can migrate from a basin to another basin.
3. The boron atom by the radical site can abstract a hydrogen atom, form a BH radical, and create a new radical site.
4. The number and distribution of open radical sites, namely, the adsorption of hydrogen atoms and the abstraction of surface hydrogen atoms, can influence the adsorption and migration of boron atoms on the hydrogen-terminated diamond surface.

Acknowledgments: The authors acknowledge the financial support provided by the National Natural Science Foundation of China (Grant Nos. 50845065 and 51562031), the Natural Science Foundation of Inner Mongolia Autonomous Region (Grant Nos. 2014MS0516, 2015MS0550, and 2015MS0554), and the Science and Technology Foundation of Baotou (Grant No.2013J2001-1).

Author Contributions: Xuejie Liu conceived and designed the researches; Congjie Kang and Haimao Qiao performed the calculations; Yuan Ren, Xin Tan, and Shiyang Sun analyzed the data and participated in the discussions; Xuejie Liu and Congjie Kang wrote the paper.

Conflicts of Interest: The authors declare no conflict of interest.

References

1. Kraft, A. Doped diamond: A compact review on a new, versatile electrode material. *Int. J. Electrochem. Sci.* **2007**, *2*, 355–385.
2. Luong, J.H.T.; Male, K.B.; Glennon, J.D. Boron-doped diamond electrode: Synthesis, characterization, functionalization and analytical applications. *Analyst* **2009**, *134*, 1965–1979. [CrossRef] [PubMed]
3. Kalish, R. Diamond as a unique high-tech electronic material: Difficulties and prospects. *J. Phys. D Appl. Phys.* **2007**, *40*, 6467–6478. [CrossRef]
4. Waldvogel, S.R.; Elsler, B. Electrochemical synthesis on boron-doped diamond. *Electrochimca Acta* **2012**, *82*, 434–443. [CrossRef]
5. Svitkova, J.; Ignat, T.; Svorc, L. Chemical modification of boron-doped diamond electrodes for applications to biosensors and biosensing. *Crit. Rev. Anal. Chem.* **2016**, *46*, 248–256. [CrossRef] [PubMed]
6. Li, L.; Li, H.D.; Lü, X.; Cheng, S.; Wang, Q.; Ren, S.; Liu, J.; Zou, G. Dependence of reaction pressure on deposition and properties of boron-doped freestanding diamond films. *Appl. Surf. Sci.* **2010**, *256*, 1764–1768. [CrossRef]
7. Zhang, J.G.; Wang, X.C.; Shen, B.; Sun, F.H. Effect of boron and silicon doping on improving the cutting performance of CVD diamond coated cutting tools in machining CFRP. *Int. J. Refract. Met. Hard Mater.* **2013**, *41*, 285–292. [CrossRef]
8. Wang, X.C.; Lin, Z.C.; Zhang, T.; Shen, B.; Sun, F. Fabrication and application of boron-doped diamond coated rectangular-hole shaped drawing dies. *Int. J. Refract. Met. Hard Mater.* **2013**, *41*, 422–431. [CrossRef]
9. Butler, J.E.; Mankelevich, Y.A.; Cheesman, A.; Ma, J.; Ashfold, M.N.R. Understanding the chemical vapor deposition of diamond: recent progress. *J. Phys. Condens. Matter* **2009**, *21*, 36–42. [CrossRef] [PubMed]
10. Frenklach, M.; Skokov, S. Surface migration in diamond growth. *J. Phys. Chem. B* **1997**, *101*, 3025–3036. [CrossRef]
11. Cheesman, A.; Harvey, J.N.; Ashfold, M.N.R. Studies of carbon incorporation on the diamond [100] surface during chemical vapor deposition using density functional theory. *J. Phys. Chem. A* **2008**, *112*, 11436–11448. [CrossRef] [PubMed]
12. Richley, J.C.; Harvey, J.N.; Ashfold, M.N.R. On the role of carbon radical insertion reactions in the growth of diamond by chemical, vapor deposition methods. *J. Phys. Chem. A* **2009**, *113*, 11416–11422. [CrossRef] [PubMed]
13. Richley, J.C.; Harvey, J.N.; Ashfold, M.N.R. CH_2 group migration between the H-terminated 2×1 reconstructed {100} and {111} surfaces of diamond. *J. Phys. Chem. C* **2012**, *116*, 7810–7816. [CrossRef]
14. Cheesman, A.; Harvey, J.N.; Ashfold, M.N.R. Computational studies of elementary steps relating to boron doping during diamond chemical vapor deposition. *Phys. Chem. Chem. Phys.* **2005**, *7*, 1121–1126. [CrossRef] [PubMed]
15. Richley, J.C.; Harvey, J.N.; Ashfold, M.N.R. Boron incorporation at a diamond surface: A QM/MM study of insertion and migration pathways during chemical vapor deposition. *J. Phys. Chem. C* **2012**, *116*, 18300–18307. [CrossRef]
16. Fang, W.H.; Peyerimhoff, S.D. Theoretical studies on mechanisms of the insertion of boron into methane and its consequent reactions. *Mol. Phys.* **1998**, *93*, 329–339. [CrossRef]
17. Das, D.; Singh, R.N. A review of nucleation, growth and low temperature synthesis of diamond thin films. *Int. Mater. Rev.* **2007**, *52*, 29–64. [CrossRef]
18. Manelli, O.; Corni, S.; Righi, M.C. Water adsorption on native and hydrogenated diamond (001) surfaces. *J. Phys. Chem. C* **2010**, *114*, 7045–7053. [CrossRef]
19. Henkelman, G.; Jóhannesson, G.; Jónsson, H. Methods for finding saddle pointsand minimum energy paths. In *Theoretical Methods in Condensed Phase Chemistry*; Schwartz, S.D., Ed.; Kluwer Academic Publishers: New York, NY, USA; Boston, MA, USA, 2002; Volume 5, pp. 269–302.

20. Ma, J.; Richley, J.C.; Davies, D.R.W.; Ashfold, M.N.R.; Mankelevich, Y.A. Spectroscopic and modeling investigations of the gas phase chemistry and composition in microwave plasma activated $B_2H_6/CH_4/Ar/H_2$ mixtures. *J. Phys. Chem. A* **2010**, *114*, 10076–10089. [CrossRef] [PubMed]
21. Mankelevich, Y.A.; Ashfold, M.N.R.; Comerford, D.W.; Ma, J.; Richley, J.C. Boron doping: B/H/C/O gas-phase chemistry; H atom density dependences on pressure and wire temperature; puzzles regarding the gas-surface mechanism. *Thin Solid Films* **2011**, *519*, 4421–4425. [CrossRef]
22. Asmussen, J.; Grotjohn, T.A.; Schuelke, T. Advances in plasma synthesis of UNCD films. In *Ultrananocrystalline Diamond: Synthesis, Properties and Applications*, 2nd ed.; Shenderova, O.A., Gruen, M.D., Eds.; Oxford: New York, NY, USA, 2012; pp. 53–83.
23. Butler, J.E.; Woodin, R.L. Thin-film diamond growth mechanisms. In *Thin Film Diamond*; Lettington, A.H., Steeds, J., Eds.; Springer Science + Business Media Dordrecht: London, UK, 1994; pp. 209–224.
24. Kresse, G.; Hafner, J. Ab initio molecular dynamics for liquid metals. *Phys. Rev. B* **1993**, *47*, 558–561. [CrossRef]
25. Kresse, G.; Furthmüller, J. Efficient iterative scheme for ab initio total energy calculation using a plane-wave basis set. *Phys. Rev. B* **1996**, *54*, 11169–11186. [CrossRef]
26. Kresse, G.; Furthmuller, J. Efficiency of ab initio total energy calculation for metals and semiconductors using a plane-wave basis set. *Comput. Mater. Sci.* **1996**, *6*, 15–50. [CrossRef]
27. Blochl, P. Projector augmented-wave method. *Phys. Rev. B* **1994**, *50*, 17953–17979. [CrossRef]
28. Kresse, G.; Joubert, D. From ultrasoft pseudopotentials to the projector augmented-wave method. *Phys. Rev. B* **1999**, *59*, 1758–1775. [CrossRef]
29. Perdew, J.P.; Burke, K.; Ernzerhof, M. Generalized gradient approximation made simple. *Phys. Rev. Lett.* **1996**, *77*, 3865–3868. [CrossRef] [PubMed]
30. Perdew, J.P.; Ruzsinszky, A.; Csonka, G.I.; Vydrov, O.A.; Scuseria, G.E.; Constantin, L.A.; Zhou, X.; Burke, K. Restoring the density-gradient expansion for exchange in solids and surfaces. *Phys. Rev. Lett.* **2007**, *100*, 136406. [CrossRef] [PubMed]
31. Monkhorst, H.; Pack, J.D. Special points for Brillouin-zone integrations. *Phys. Rev. B* **1976**, *13*, 5188–5192. [CrossRef]
32. Liu, X.J.; Zhang, S.H.; Jiang, Y.J.; Ren, Y. Interface structure of nanodiamond composite films: First-principles studies. *J. Alloys Compd.* **2014**, *599*, 183–187. [CrossRef]
33. Kittel, C. *Introduction to Solid State Physics*, 8th ed.; John Wiley & Sons Inc.: New York, NY, USA, 2005; p. 59.